DOI: 10.13009/EUCASS2019-657

Design of an On-board Flight Safety System for Space Microlaunch Vehicles

C. Pou, D. Vallverdú**, E. Diez****
GTD, 17 Passeig Garcia Faria (08005 Barcelona, Spain)
**carles.pou@gtd.eu; **david.vallverdu@gtd.eu; ***eduard.diez@gtd.eu*

Abstract

The growth of the microlaunch market is breaking the relationship paradigm between a spaceport and launch services operated by a single organization. Microlaunch services initiatives are planning to launch from more than one spaceport to reach the necessary launch rate to succeed in their business plan goals. Simultaneously, spaceports are preparing themselves to be able to provide base services to multiple launch concepts (vertical, horizontal, reusable, airborne…) operated by different private organizations. In such scenario, standard and modular systems, which contribute to cost-effectiveness, responsiveness and flexibility of the launch campaigns, are becoming essential for both microlaunch service providers and spaceports to achieve launch rate and cost fitting the payload market.

The on-board flight safety system (OBFS) of the launcher avionics provides the embedded real-time safety algorithms with a single standard interface with ground stations devoted to mission tracking. Considering the OBFS to be a tested and validated standard equipment, its integration in the launcher allows for the optimization of ground operations and infrastructures, radar stations in particular, by first reducing the pre-flight phase dedicated to mission configuration, equipment preparation and safety operators training; and secondly providing autonomous real-time operations devoted to the processing of tracking means and safety decision making.

The present work is in the frame of the ALTAIR H2020 project, devoted to the design of an airborne launch service concept. This paper is focused on the architecture and algorithms of the OBFS on-board the ALTAIR avionics. The architecture is based on two major components: the navigation module, based on GNSS-IMU hybridization, and the safety assessment module. The objective is to validate the performance (reliability, precision and availability) of the safety module serviced by a light-weight and cost-effective navigation system in the critical operational scenarios identified for an airborne concept: the carrier manoeuvre to initialise the launcher navigation system, the release consent procedure, the ignition consent after release and the ascend flight timeline.

The critical algorithms covering the abovementioned functions are in the frame of state estimation, filtering and propagation. Two main algorithms are implemented and tested: the impact area of a ballistic fall based on the F&G Series concept for state uncertainty propagation and the attitude propagation of the rocket free flight, based on Runge-Kutta propagation of attitude and attitude rate state. The impact area algorithm provides safety criteria for the release consent and the nominal ascent flight considering the safety of people and goods in case of launcher failure leading to a neutralisation or uncontrolled descent trajectory. The attitude propagation provides safety decision making for ignition consent procedure in degraded release scenarios. The OBFS architecture is tested in nominal and degraded mission scenarios with two objectives: the characterization of the system operational frame limits through a sensitivity analysis and the validation of safety outputs with respect to operational safety standards. The results of the present study contribute to the airborne system definition loop (alignment manoeuvre, release system, launcher aerodynamics) and provide real-time safety operations scenario awareness.

1 Context

The market for payload launchers is always driven by user needs downstream. The downstream users and the end users ultimately determine the: size (mass), type of payload, orbit, potential payload configuration etc. Therefore, to get a good picture of what the market for a European spaceport is, there is an intrinsic need to delve into the types of payloads that will be launched. The below diagram shows the global predicted payload market for the next 10 years distributed by orbit and begins to paint a global picture of which payloads will be needed in the next 10 years. The diagram has been driven from the payload operators themselves rather than the launch services to show how many payloads will be launched [1].

DOI: 10.13009/EUCASS2019-657

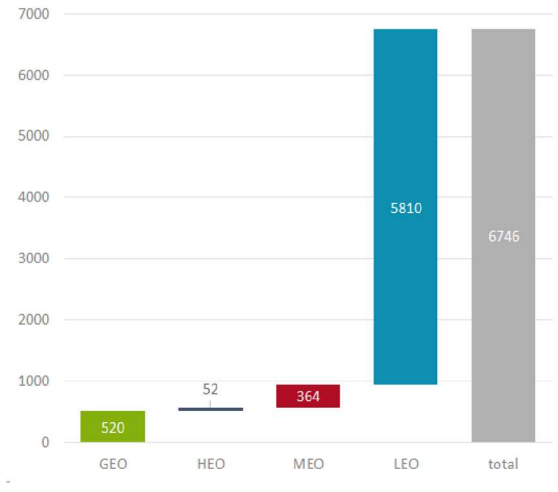

Figure 1: 10 Year Global Satellite Launch Forecast by Orbit [Euroconsult and ICS]

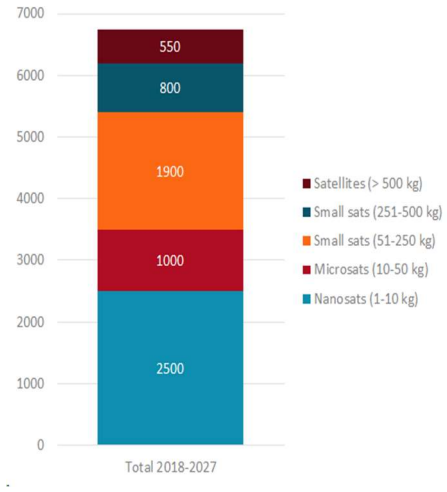

Figure 2: 10 Year Global Satellite Launch Forecast by Mass [Euroconsult and ICS]

The worldwide payload market is experiencing a significant growth period and shows no sign of slowing down, however reliability and reactivity are increasingly becoming important factors launch requirements. With these upcoming launches, the payload and launch vehicle market is expected to keep expanding. This paper addresses this fact by specifically targeting the small launcher costs and their demands, low cost, versatility and standardisation. The growing demands of the payload segment will necessitate dedicated, cost-effective high launch rates which satisfy their stringent economics constraints. This is evident with almost 20% of the demand coming from Europe in the next 10 years. This is particularly important for payload constellations, which demand accurate orbit injections to maintain their cash flow. As a consequence, the key drivers for these new launch services are cost, launch frequency, mission availability, flexibility and responsiveness [2].

The costs of building spaceports are also very high, so these need to be amortised by many launches. The way to achieve this is to be open spaceports to host as many launchers as possible and design launchers that can put payloads into orbit from multiple spaceports. To succeed in such scenario of multiple launch concepts –to- multiple launch sites in a private market, launcher systems and launch sites need the contribution of all systems and subsystems to the overall goals of:

1. Reduce complexity, with a focus on infrastructures compactness, modularity and standardization.
2. Increase availability and maintainability while reducing operational risks, bringing both an increase in launch frequency and a reduction in costs.
3. Increase agility by providing higher schedule flexibility, reducing inter-campaign preparation time, sustaining a high launch rate and enhancing mission responsiveness. This allows for an economy of scale in launch vehicle production and ground systems operations, reducing overall costs.

Three points above contribute to major goals of the future launch market: affordable cost and high launch rate to help enabling the space business case. The avionics subsystem tackles the challenge in different axes as shown in Figure 3.

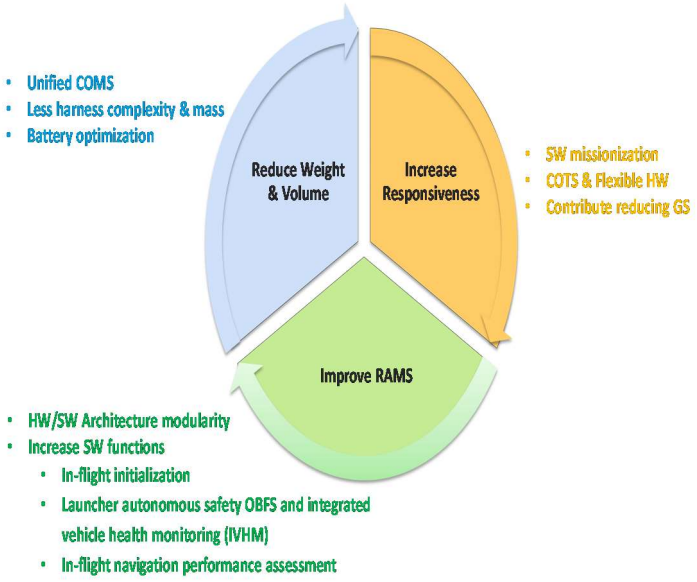

Figure 3: Avionics axes of improvement

DOI: 10.13009/EUCASS2019-657

As part of the avionics, the concept of an Autonomous On-board flight Safety system is identified (AOBFS), or autonomous flight Safety system (AFSS) as one of the potential contributors to the future launch system goals [9]. The AOBFS allows the evaluation of safety scenarios and the decision making of safety actions without the telemetry and human chain on ground. Therefore the system helps:

- Reducing drastically the infrastructures, personnel and operations devoted to safety in real-time tracking operations, primary radars
- Reducing training operations during mission preparation
- Making agile mission submission process, which could be realized automatically
- Agile intercampaign validation operations through SW on-board missionization for different missions and launch systems

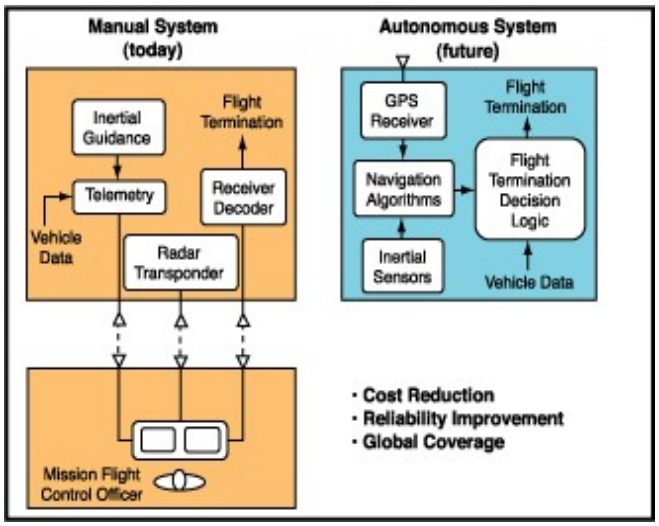

Figure 4: Traditional versus autonomous flight safety systems

The objective of the present papers is to assess and evaluates the contribution of the AOBFS to the space scenario described above regarding the goals in terms of cost, flexibility, launch rate and safety requirements, such precision for decision making. The work described in this paper seeks the characterization of the operational frame of an autonomous on-board flight safety standard and modular through missionization

Next section 2 describes the architecture of the on-board SW including safety subsystem and navigation subsystem, providing the main input for the safety algorithms in real-time. Section 3 describes in detail the safety algorithms. After the presentation of the subsystem, section 4 presents the sensitivity study applied to the safety and navigation subsystem to assess the performance in operational mission, in nominal and non-nominal scenarios, of different configurations of safety subsystem.

The study presented in this paper is based on the work developed in frame of the ALTAIR project (Air Launch space Transportation using an Automated aircraft and an Innovative Rocket), which strategic objective is to demonstrate the economic and technical viability of a future available, reliable and competitive European launch service for the access to space (Low-Earth Orbit) of nano and micro satellites [8]. ALTAIR is an innovative semi-reusable air-launch system consisting of a reusable unmanned aircraft carrier, an expendable rocket launch vehicle and a cost-effective ground segment. Its reference mission is to carry 150 kg of payload(s) to a sun-synchronous orbit at 600 km. The mission profile expects the carrier takes-off from the ground bringing the rocket vehicle at the right altitude, drops it and comes back to the ground for further reuse. After releasing, the launch vehicle boosts the payload over its operational orbit.

2 On-board flight safety system design

2.1 Design points

Since the beginning of the Space Age in the 1960s, flight safety systems of rocket launch vehicles have traditionally been ground-based. The function of these systems include tracking the vehicle with precision radars; monitoring its progress through telemetry; using high-powered transmitters to send, if necessary, neutralization commands to on-board receivers; and ensuring the protection of the environment through the compliance of international environmental laws. All these actions require highly reliable, redundant systems dependent on line-of-sight radio frequency transmissions. Additionally, these systems need dedicated maintenance and operation —often at isolated locations.

DOI: 10.13009/EUCASS2019-657

The avionics include the concept of an autonomous flight safety module on-board the rocket. This decision seeks to minimize the human factor in the decision-making process as well as simplify the requisites and needs of ground segment. It has been driven by the awareness that the availability of an autonomous, on-board flight abort/flight termination system has numerous benefits. For instance:

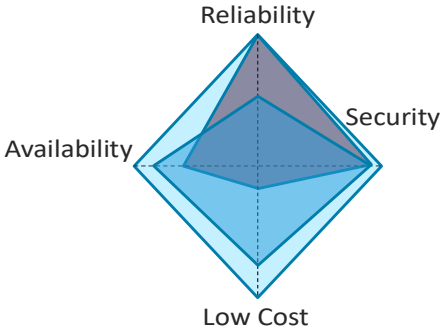

Figure 5: Flight Safety for legacy launchers (grey) vs on-board flight safety (blue)

- It enhances operational margins for safe flight abort or termination by reducing the total decision delays,
- It increases flight termination reliability by eliminating radio links and reducing the total number of involved hardware equipment in the decision chain,
- It increases flight termination reaction time (safety procedure responsiveness),
- It ensures global operations coverage where range safety ground installations may not be available, and
- It reduces maintenance and operation costs by streamlining ground segment complexity and mission preparation (mission responsiveness and missionization)

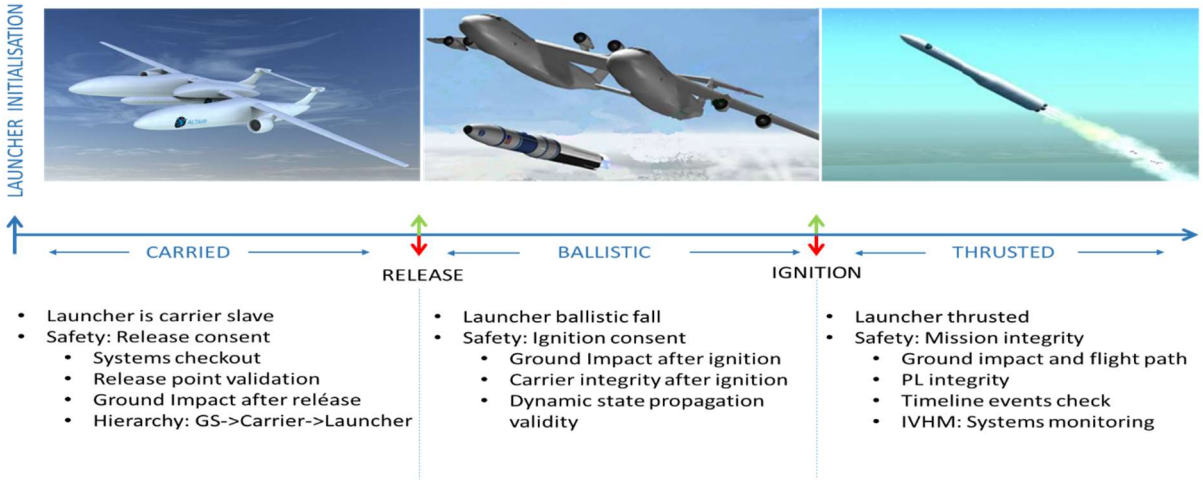

Figure 6: Safety requirements for air-born launch concept

The definition of the on-board flight safety architecture, as well as the roles of its components, is based on a preliminary analysis of the mission phase's requirements. The scenarios studied in this paper consider the carried and the ballistic phase:

Carried phase: The avionics system is responsible for the launcher status checkout after in-flight initialization. This procedure encompasses:

- The verification of the launcher's systems status
- The instantaneous impact point prediction to ensure ground safety in case of any degrade scenario that would lead to a launcher switch-off or drop
- the verification of the launch acceptability region (LAR) based on the launcher's dynamic state
- The release consent dialog with the carrier
    - Nominal release of the launcher: launcher status ok and nominal release point reached at nominal dynamic conditions
    - Non-nominal non-critical scenario: Carried launcher re-entry to base

Ballistic phase: This is the most vulnerable and critical period of the mission with regards to the safety system and its role in evaluating the launcher's dynamics since neither thrust control nor AOCS are available to mitigate perturbations on the launcher. During this phase, the safety system monitors the launcher's dynamic state and prevents first ignition under degraded dynamic conditions that would compromise ground safety, the carrier's integrity, or mission success. Throughout the ballistic fall, the decision-making hierarchy –from highest to lowest authority— consists of ground

segment, followed by the launcher. Therefore, the launcher decides, under segment ground supervision, if it begins

- Nominal ignition at nominal time and conditions, or
- Launcher passivation (switch-off, propellant jettison).

The AOBFS is responsible for:

- Identify launcher and mission status,
- Ensuring a minimum success rate of the mission,
- Protecting the populated areas, properties, the carrier and the payload.
- Protecting the environment

2.2 System architecture

The module is embedded in the Safety OBC placed in the upper stage of the launcher. Based on the design principles in the previous section, the AOBFS architecture is composed by the following modules, from the range-centric, vehicle-centric, and IVHM approaches:

- Ground Safety analyzer: This function assess the safety of people and goods on ground using propagated impact points and impact areas
    - An instantaneous impact point (IIP) and area (IIA) prediction algorithm responding to range centric approaches;
    - Intersection Calculator
    - Identity re-entry zones: Identify the safety of sensitive regions on Earth from impact point/area computations. This includes both regions to be avoided and regions to be targeted.
    - Predict impact area: Predict the n-σ area that corresponds to the calculation of an impact point on Earth.
    - Predict impact point: Predict the impact point on Earth of a flying object given its position and velocity at a certain instant of time.
- In-flight Safety analyzer: This function diagnoses the safety status of the flight, in terms of nominal flight path.
    - An identification of the launcher's dynamic state and its propagation, responding to vehicle centric approaches; and
    - A measure of the launcher's flight path and trajectory integrity given its current or future dynamic state.
    - The diagnosis module shall evaluate at current time launcher dynamics adequacy wrt nominal launch dynamics
    - The diagnosis module shall evaluate launcher dynamics wrt nominal launcher dynamics at propagated time
    - The diagnosis module shall propagate the trajectory of the launcher
    - The diagnosis module shall be able to identify a non-nominal dynamics of the launcher
- Vehicle Safety Analyzer:

  An IVHM module that performs diagnostics of the launcher and PL concerning non-critical data for safety. In doing so, it provides system status awareness during the mission, which may eventually become useful to evaluate the integrity of the mission
- Safety scenario awareness, including
    - Safety Criteria Evaluator: the evaluation of all diagnostic and safety data internally generated, this function processes all the individual diagnostics reports into a unified diagnosis solution for safety criteria evaluation

DOI: 10.13009/EUCASS2019-657

- Safety Decision making: in function of the safety criteria, this-function evaluates the diagnosis solution in order to make a safety decision

- AOBFS interfaces
  - External: Communications with carrier, ground telecommand
  - Internal:
    - with avionics equipment towards IHVM
    - with OBC
    - with navigation instruments devoted to safety

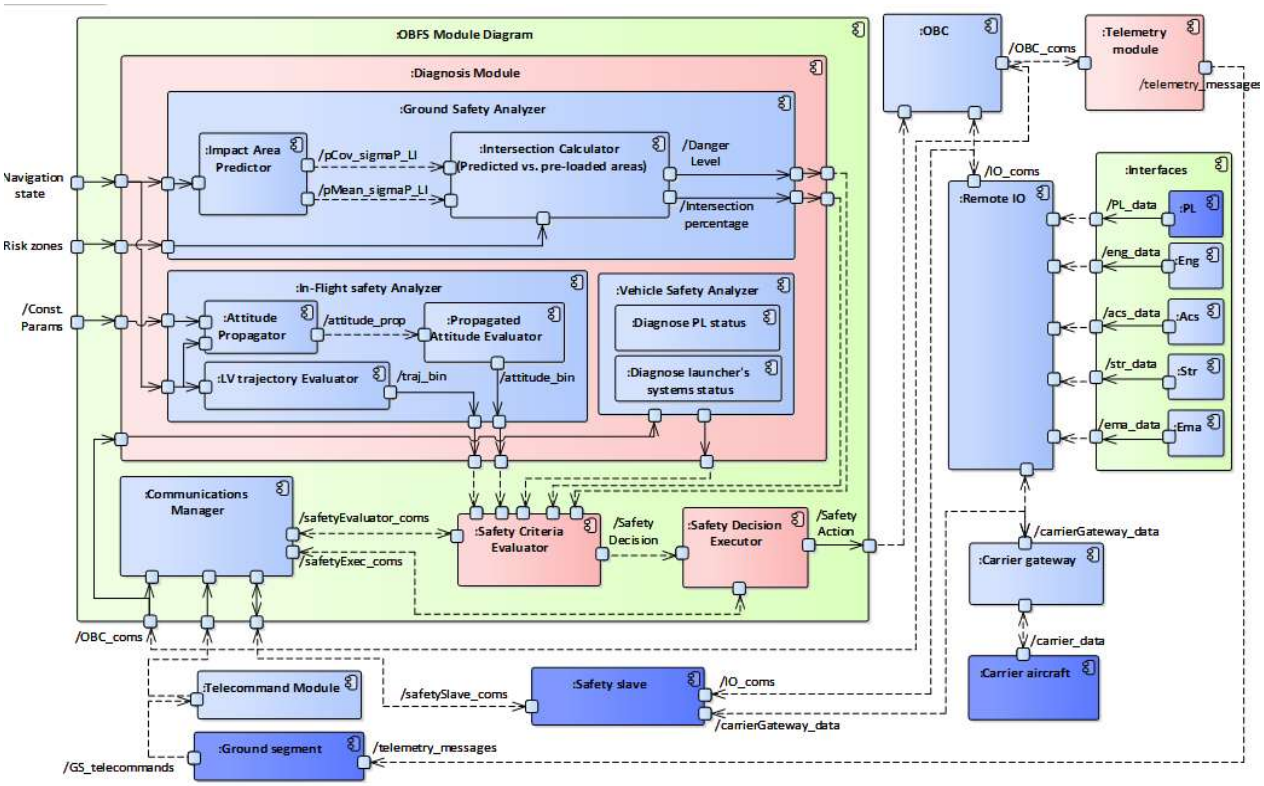

Figure 7: AOBFS architecture

The Navigation module provides with the necessary information to the safety algorithms from launcher dynamic state. The Safety Module performance is strongly dependant from the performance of the navigation module. The navigation subsystem cannot be therefore be dissociated from the sensitivity analysis of the AOBFS developed in section 4 over algorithms in section 3, with the objective of validating the AOBFS approach with respect to launch system goals.
The sensitivity study includes therefore a Safety subsystem run over a set of navigation architecture configurations and over a set of navigation scenarios, nominal and degraded, in order to assess the operational performance of the AOBFS.

3 Real-time safety algorithms

3.1 Navigation system

The navigation architecture is based under main hypothesis [3] of a launcher switched on and initialized in-flight with negligible multi-path effect. The interfaces and components involved in the study are:

- Navigation Module Interfaces, defining a scenario:
  - Inputs:
    - Navigation instruments: the objective is to characterize and design launcher navigation instruments performances in terms of accuracies, frequencies, availabilities and ranges in the nominal navigation and in-flight alignment scenarios

- Launcher Inertial Measurement Unit: attitude and attitude rate
- Launcher GNSS receiver: position and velocity

  - Carrier dynamic data interface in terms of accuracies, frequencies, availabilities and ranges during in-flight alignment scenario maneuver

- Outputs:
  - Guidance Module: estimated launch vehicle position and velocity expected requirements
  - Control Module: estimated attitude and attitude rate for control algorithm expected requirements

Launch vehicles targeting PL between 50-500 Kg aims to use COTS equipment for navigation instruments in order to safe cost, mass and volume. To avoid losing performance due to COTS instruments, navigation solution is based on hybridation approaches, fusing data from a low-end Inertial Measurement Unit (IMU) and a Global Navigation Satellite System (GNSS). Because the embedded systems of the SLV boot up during captive flight, a transfer alignment is needed to initialize the hybrid navigation [6], [7]. Figure 8 shows the resulting architecture. The two navigation modules have different prominence depending on the phase of the mission:

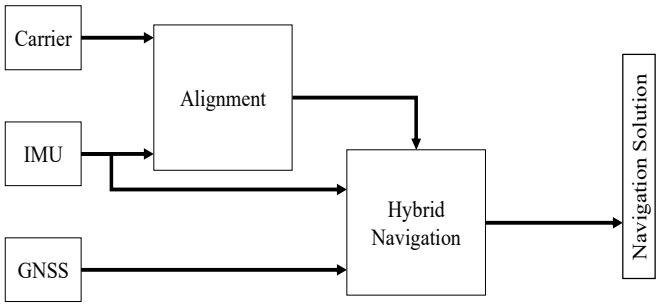

Figure 8: Navigation architecture

- During captive flight, after avionics initialization, the SLV uses carrier navigation data and its own IMU to align its navigation.
- Upon release of the SLV from the carrier, the alignment module transfers the aligned navigation state to the hybrid navigation module.
- After SLV release, the already initialized hybrid navigation continuously provides a navigation solution by hybridizing on-board IMU and GNSS sensors.

Main hybrid navigation techniques involve the use of Kalman filters. They can be divided into profile-based and profile-free. On the one hand, profile-based implementations use a dynamic state model that increases the accuracy of the estimation when the vehicle trajectory fits the model, but fail when it does not. On the other hand, profile-free implementations make no assumptions on the type of trajectory that the vehicle follows –this approach can be used for a wider range of trajectories, but performs worse than a well matched profile-based method of the same computational order. The potential navigation filters considered for use in the SLV are a profile-free Extended Kalman Filter (EKF) [4] and a profile-free Indirect Kalman Filter (IKF) that uses a linearized state-error model [6] [11].

3.1.1 Alignment

Alignment is the process by which the initial state (position, velocity and attitude) of an inertial navigation system is determined [9]. This is most critical in IMU-only systems, in which alignment errors can totally define their performance throughout the whole mission. The SLV hybrid navigation system can absorb some initial error thanks to GNSS measurements, at the cost of a transient phase in which navigation errors are above nominal level. However, while the SLV is captive, GNSS signal may be unavailable due to carrier interference. Therefore, a transfer-alignment process before release is still desirable so that pre-release safety assessment algorithms have accurate navigation data at their disposal – these are the most critical users of the navigation output.

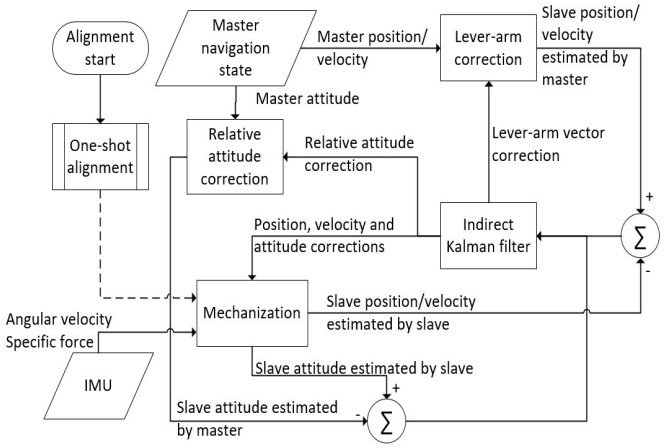

Figure 9: Transfer alignment diagram starting from (dotted line) a one-shot initialization of the Mechanization process

DOI: 10.13009/EUCASS2019-657

Given that SLV embedded systems initialize during captive flight, alignment happens in a non-stationary environment. The strategy used, known as transfer alignment, involves the carrier (*aka* master) transferring its own navigation data to the SLV (*aka* slave) during captive flight (Figure 9). For this data transfer to be useful for SLV alignment purposes, the carrier simultaneously needs to perform a certain manoeuvre that dynamically stimulates the IMU on-board the SLV. A profile-free Indirect Kalman Filter (IKF) [9] matches carrier navigation data (position, velocity, attitude or a combination of these) with SLV IMU measurements via a linearized model of the alignment error [6] [7].

3.1.2 Hybrid navigation

Upon release of the SLV, the navigation solution provided by the alignment process is transferred to the hybrid navigation module, which fuses data from IMU and GNSS sensors to continue to provide a reliable navigation solution without transient errors. Figure 10 depicts this process. An Extended Kalman Filter (EKF) is used to continuously update the navigation solution, which becomes available to all navigation users (e.g. safety algorithms, GNC, telemetry, etc.).

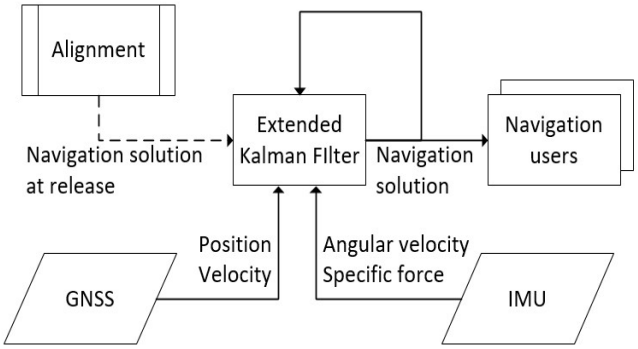

Figure 10: Hybrid navigation diagram initializing the EKF with the alignment navigation solution (dotted line).

The state of the EKF is given by [15]

$$\vec{\boldsymbol{x}} = \left[\vec{\boldsymbol{r}}^{\boldsymbol{i}^T} \quad \vec{\boldsymbol{v}}^{\boldsymbol{i}^T} \quad \boldsymbol{f}^{\boldsymbol{i}^T} \quad \vec{\boldsymbol{\omega}}_{\boldsymbol{ib}}^{\boldsymbol{b}\ T} \quad \boldsymbol{\Psi}_{\boldsymbol{i}}^{\boldsymbol{b}^T}\right]^{\boldsymbol{T}}, \quad \textbf{(1)}$$

where $\vec{r}^i$ and $\vec{v}^i$ are respectively the position and velocity of the SLV in the ECI frame, f^i is the specific force[1] received by the SLV (also in ECI), $\vec{\omega}_{ib}^{\ b\ T}$ is the angular velocity expressed in the body frame (attached to the SLV) of the SLV around ECI, and Ψ_i^b represents the 3-2-1 Euler angles that transform from ECI to the body frame. The EKF propagates the state from one time-step to the next with the model:

$$\begin{gathered}
\vec{\boldsymbol{r}}^{\boldsymbol{i}}(\boldsymbol{t}+\boldsymbol{\Delta t}) = \vec{\boldsymbol{r}}^{\boldsymbol{i}}(\boldsymbol{t}) + \vec{\boldsymbol{v}}^{\boldsymbol{i}}(\boldsymbol{t})\boldsymbol{\Delta t} + \left(\vec{\boldsymbol{f}}^{\boldsymbol{i}}(\boldsymbol{t}) + \vec{\boldsymbol{g}}^{\boldsymbol{i}}(\boldsymbol{t})\right)\frac{\boldsymbol{\Delta t^2}}{\boldsymbol{2}}\ ; \\
\vec{\boldsymbol{v}}^{\boldsymbol{i}}(\boldsymbol{t}+\boldsymbol{\Delta t}) = \vec{\boldsymbol{v}}^{\boldsymbol{i}}(\boldsymbol{t}) + \left(\vec{\boldsymbol{f}}^{\boldsymbol{i}}(\boldsymbol{t}) + \vec{\boldsymbol{g}}^{\boldsymbol{i}}(\boldsymbol{t})\right)\boldsymbol{\Delta t}\ ; \\
\vec{\boldsymbol{f}}^{\boldsymbol{i}}(\boldsymbol{t}+\boldsymbol{\Delta t}) = \vec{\boldsymbol{f}}^{\boldsymbol{i}}(\boldsymbol{t})\ ; \vec{\boldsymbol{\omega}}_{\boldsymbol{ib}}^{\boldsymbol{b}}(\boldsymbol{t}+\boldsymbol{\Delta t}) = \vec{\boldsymbol{\omega}}_{\boldsymbol{ib}}^{\boldsymbol{b}}(\boldsymbol{t})\ ; \qquad \textbf{(2)} \\
\vec{\boldsymbol{\Psi}}_{\boldsymbol{i}}^{\boldsymbol{b}}(\boldsymbol{t}+\boldsymbol{\Delta t}) = \vec{\boldsymbol{\Psi}}_{\boldsymbol{i}}^{\boldsymbol{b}}(\boldsymbol{t}) + \boldsymbol{\Delta t}\begin{bmatrix} \boldsymbol{\omega_x} + \left(\sin\boldsymbol{\phi}\,\boldsymbol{\omega_y} + \cos\boldsymbol{\phi}\,\boldsymbol{\omega_z}\right)\tan\boldsymbol{\theta} \\ \left(\cos\boldsymbol{\phi}\,\boldsymbol{\omega_y} - \sin\boldsymbol{\phi}\,\boldsymbol{\omega_z}\right) \\ \left(\sin\boldsymbol{\phi}\,\boldsymbol{\omega_y} + \cos\boldsymbol{\phi}\,\boldsymbol{\omega_z}\right)\sec\boldsymbol{\theta} \end{bmatrix}
\end{gathered}$$

The following notation has been used: $\vec{\omega}_{ib}^{b}(t) = [\omega_x \quad \omega_y \quad \omega_y]$ and $\vec{\Psi}_i^b(t) = [\phi \quad \theta \quad \psi]$. The measurement model estimates the IMU and GNSS measurements from the state as [14]:

$$\vec{\boldsymbol{r}}_{\boldsymbol{GPS}}^{\boldsymbol{i}} = \boldsymbol{r}^{\boldsymbol{i}}\ ;\ \vec{\boldsymbol{v}}_{\boldsymbol{GPS}}^{\boldsymbol{i}} = \boldsymbol{v}^{\boldsymbol{i}}\ ;\ \vec{\boldsymbol{f}}_{\boldsymbol{IMU}}^{\boldsymbol{b}} = \boldsymbol{C}_{\boldsymbol{i}}^{\boldsymbol{b}}\vec{\boldsymbol{f}}^{\boldsymbol{i}}\ ;\ \vec{\boldsymbol{\omega}}_{\boldsymbol{ib\,IMU}}^{\boldsymbol{b}} = \vec{\boldsymbol{\omega}}_{\boldsymbol{ib}}^{\boldsymbol{b}}\,. \qquad \textbf{(3)}$$

Note that the matrix C_i^b is the rotation matrix from ECI to body frame, which can be calculated from Ψ_i^b [4] [5]

3.2 Safety

3.2.1 Ground safety

3.2.1.1 Impact Point

The Ground Safety Analyser (GSA) uses the navigation position and velocity to predict the point on the Earth's surface where the launcher would fall should it not ignite after release –i.e. in case it performed a free fall. This point is used afterwards to compute an impact area, by including the uncertainties of the model. Because this propagation occurs much farther away in the future than the FSA, the GSA does not propagate attitude, and does not use RK4. Instead, the propagator is an expansion of the F&G Series. This method is based on the Taylor decomposition of [12]

$$\vec{\boldsymbol{r}}^{\boldsymbol{i}}(\boldsymbol{t}+\boldsymbol{\Delta t}) = \sum_{\boldsymbol{n}=\boldsymbol{0}}^{+\infty}\frac{\boldsymbol{\Delta t^n}}{\boldsymbol{n!}}\frac{\boldsymbol{d^n}\vec{\boldsymbol{r}}^{\boldsymbol{i}}}{\boldsymbol{dt^n}}\bigg|_{\boldsymbol{t_0}} \qquad \textbf{(4)}$$

[1] Specific force is the acceleration due to non-conservative forces, such as thrust, aerodynamic loads, etc...

and the fact that each term of the Taylor series can be expressed as

$$\frac{1}{n!}\frac{d^n\vec{r}^i}{dt^n} = f_n\vec{r}^i + g_n\frac{d\vec{r}^i}{dt} + h_n\vec{v}^i + i_n\frac{d\vec{w}^i}{dz}, \tag{5}$$

where

$$\vec{v}^i = \frac{d\vec{r}^i}{dt} - \vec{\Omega}_E^i \times \vec{r}^i - \vec{w}^i \tag{6}$$

is the velocity of the SLV relative to the air in ECI, $\vec{\Omega}_E^i$ is the inertial angular rotation of the Earth in ECI, $\vec{w}^i$ is the wind speed relative to the Earth in ECI, and z is the altitude of the SLV. The wind speed depends only on the altitude, and any model shall be used. The coefficients f_n, g_n, h_n and i_n for $n \geq 2$ can be deduced by derivation of the dynamic model

$$\frac{d^2\vec{r}^i}{dt^2} = \left(\frac{d^2\vec{r}^i}{dt^2}\right)_G + \left(\frac{d^2\vec{r}^i}{dt^2}\right)_A = -\frac{\mu}{\|\vec{r}^i\|^3}\vec{r}^i - \frac{\rho\|\vec{v}^i\|}{2\beta}\vec{v}^i . \tag{7}$$

Here, β is the SLV ballistic coefficient and ρ is the air density. Thus, the position can be propagated by using

$$\begin{aligned} \vec{r}^i(t_0 + \Delta t) &= f\vec{r}^i + g\frac{d\vec{r}^i}{dt} + h\vec{v}^i + i\frac{d\vec{w}^i}{dz} \text{ and} \\ \frac{d\vec{r}^i}{dt}(t_0 + \Delta t) &= \frac{df}{d\Delta t}\vec{r}^i + \frac{dg}{d\Delta t}\frac{d\vec{r}^i}{dt} + \frac{dh}{d\Delta t}\vec{v}^i + \frac{di}{d\Delta t}\frac{d\vec{w}^i}{dz}, \end{aligned} \tag{8}$$

where

$$f = \sum_{n=0}^{+\infty} f_n\Delta t^n ;\ g = \sum_{n=0}^{+\infty} g_n\Delta t^n ;\ h = \sum_{n=0}^{+\infty} h_n\Delta t^n ; i = \sum_{n=0}^{+\infty} i_n\Delta t^n . \tag{9}$$

3.2.1.2 *Impact area*

The impact area of the launcher on ground is calculated in two ways:

- With a linear method: The safety system evaluates each point of the trajectory as follows: it runs the F&G series to obtain the covariance matrix of the position and velocity at impact, uses the position components of this matrix to generate a two-dimensional ellipse representing the error in latitude and longitude at impact, and calculates the area of the figure to find an estimate of the area of the impact zone.
- With a nonlinear method: For each vector state of the launcher's trajectory, the safety system uses the Scaled Unscented Transform (SUT) to compute the coordinates of $(2n + 1)$ sigma points, propagate them with the F&G series, and calculate the mean and covariance of the sigma-point distribution from a weighted average of the transformed points. The covariance is then used to represent a 95% confidence error ellipse.

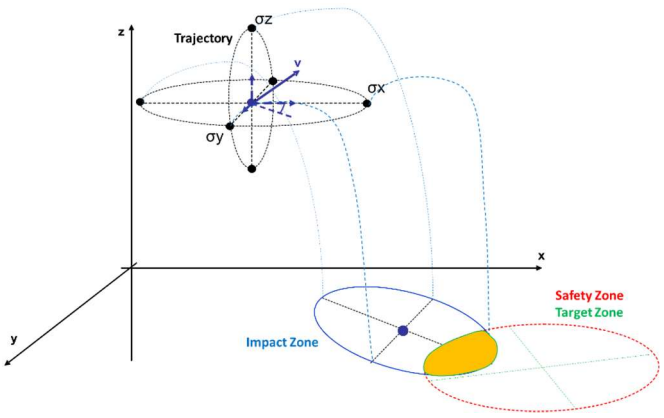

Figure 11: Impact area diagnostic criteria

The first estimate of the impact area derives from the F&G series: upon calculating the position and velocity at impact, the code returns the covariance matrix of such variables, obtained by linearly propagating the initial covariance matrix to the impact point. The F&G series only propagates an initial state

$$\vec{x} = \begin{bmatrix} \vec{r} \\ \frac{d\vec{r}}{dt} \end{bmatrix} \tag{10}$$

from t_0 to $t = t0 + \Delta t$:

$$x(t) = f_{FG}(x(t_0), t) . \tag{11}$$

If one assumes that the f, g, h and i coefficients are constant within $[t_0, t]$, one can compute the state transition matrix [4] as

DOI: 10.13009/EUCASS2019-657

$$\boldsymbol{\Phi(t_0,t)} = \left.\frac{\partial \boldsymbol{f_{FG}}}{\partial \boldsymbol{x}}\right|_{x(t_0)} = \begin{bmatrix} \boldsymbol{fI_3} & \boldsymbol{gI_3} \\ \boldsymbol{f'I_3} & \boldsymbol{g'I_3} \end{bmatrix} + \begin{bmatrix} \boldsymbol{0} & \boldsymbol{\frac{\Delta t^3}{6}j} \\ \boldsymbol{0} & \boldsymbol{\frac{\Delta t^2}{2}j} \end{bmatrix} + \begin{bmatrix} \boldsymbol{-h[\omega\times]} & \boldsymbol{hI_3} \\ \boldsymbol{-h'[\omega\times]} & \boldsymbol{h'I_3} \end{bmatrix}. \tag{12}$$

If $\vec{q}$ and $d\vec{q}/dz$ are interpreted as process noise (one may not know exactly how the wind shall change with altitude in a realistic scenario, the error transition matrix becomes

$$\boldsymbol{\Gamma(t_0,t)} = \begin{bmatrix} \boldsymbol{-hI_3} & \boldsymbol{iI_3} \\ \boldsymbol{-h'I_3} & \boldsymbol{i'I_3} \end{bmatrix} \tag{13}$$

Thus, the error in the state, assuming it is linear, can be propagated as

$$\boldsymbol{\delta x(t)} = \boldsymbol{\Phi(t_0,t)\delta x(t_0)} + \boldsymbol{\Gamma(t_0,t)} \begin{bmatrix} \boldsymbol{\delta\vec{q}} \\ \boldsymbol{\delta\frac{d\vec{q}}{dz}} \end{bmatrix}. \tag{14}$$

Being P_x the covariance of the error in the state,

$$\boldsymbol{P_x} = \boldsymbol{E(\delta x \delta x^T)}\,, \tag{15}$$

It can be propagated as

$$\boldsymbol{P_x(t)} = \boldsymbol{\Phi P_x(t_0)\Phi^T + \Gamma Q \Gamma^T}\,, \tag{16}$$

where Q is the covariance of the process noise, if assumed to be Gaussian.

$$\boldsymbol{Q} = \begin{bmatrix} \boldsymbol{E(\delta\vec{q}\delta\vec{q}^T)} & \boldsymbol{0} \\ \boldsymbol{0} & \boldsymbol{E\left(\delta\frac{d\vec{q}}{dz}\delta\frac{d\vec{q}^T}{dz}\right)} \end{bmatrix}. \tag{17}$$

The second method used to calculate the launcher's impact area on ground is the Scaled Unscented Transformation (SUT). Given a non-linear transformation $\boldsymbol{y = f(x), x \sim X, y \sim Y}$, the SUT is able to transform the covariance from the space $\boldsymbol{X}$ to space $\boldsymbol{Y}$ with an accuracy that varies from second to fourth order error, depending on the tuning parameters of the SUT and the statistical distribution $\boldsymbol{X}$. Also, the SUT is a generic method that does not need to know the derivatives of $\boldsymbol{f}$. Instead, it stores the covariance information in a set of carefully chosen sample points of the original distribution, and recovers it after transforming each point with $\boldsymbol{f}$.

3.2.2 In-flight safety: Attitude propagation

The Flight Safety Analyser (FSA) uses the navigation solution (i.e. position, velocity and attitude) and the angular velocity computed by the gyroscope to predict the attitude in the near future. To this end, the FSA propagates the state

$$\vec{x} = \begin{bmatrix} \vec{r}^{\,iT} & (d\vec{r}^{\,i}/dt)^T & \vec{q}_b^{\,i\,T} & \vec{\omega}_{ib}^{\,b\,T} \end{bmatrix}^T \tag{18}$$

through time by integrating the system

$$\frac{d\vec{x}}{dt} = \left[\left(\frac{d\vec{r}^{\,i}}{dt}\right)^T \quad \left(\frac{\vec{F}_a^{\,i}}{m} - \frac{\mu}{\|\vec{r}^{\,i}\|^3}\vec{r}^{\,i}\right)^T \quad \left(\frac{1}{2}\Omega\vec{q}_b^{\,i}\right)^T \quad \left(I^{-1}\left(\sum\vec{M}_{CG} - \vec{\omega}_{ib}^{\,b} \times \left(I\vec{\omega}_{ib}^{\,b}\right)\right)\right)^T \right]^T \tag{19}$$

using a classic Runge-Kutta of order 4 (RK4) [13]. In the above equation, t is time, μ is the Earth's gravitational constant, $\vec{r}^{\,i}$ is the position of the SLV in Earth Centred Inertial (ECI) frame, $\vec{q}_b^{\,i}$ is the quaternion[2] that transforms from body frame (attached to the SLV) to ECI frame, $\vec{\omega}_{ib}^{\,b}$ is the angular velocity of the SLV around ECI in body frame, $\boldsymbol{I}$ is the inertia tensor of the SLV in body-frame, $\boldsymbol{\Omega}$ is the quaternion multiplication matrix

$$\boldsymbol{\Omega} = \begin{bmatrix} -\left[\vec{\omega}_{ib}^{\,b}\times\right] & -\vec{\omega}_{ib}^{\,b} \\ \vec{\omega}_{ib}^{\,b\,T} & 0 \end{bmatrix} \tag{20}$$

used to compute the variation of the quaternion with time [10], and $\vec{F}_a^{\,i}$ and $\sum\vec{M}_{CG}$ are respectively the aerodynamic force and torque experienced by the SLV in its centre of gravity (CG). The latter are function of velocity, as well as of the geometric characteristics of the launcher (i.e. lift and drag coefficient, distance from CG to center of pressure CP, cross-section area and fin area).

[2] By convention in this paper, quaternions expressed in vector form $\vec{q} = [q_1 \quad q_2 \quad q_3 \quad q_4]^T$ correspond to the hypercomplex number $\boldsymbol{q} = q_4 + q_1\boldsymbol{i} + q_2\boldsymbol{j} + q_3\boldsymbol{k}$, where $\boldsymbol{i^2 = j^2 = k^2 = -1}$, $\boldsymbol{ij = -ji = k}$, $\boldsymbol{jk = -kj = i}$ and $\boldsymbol{ki = -ik = j}$. Likewise, a rotation quaternion $\boldsymbol{q}_a^b$ in vector form is $\vec{q}_a^{\,b} = [(\vec{e}\sin(\phi/2))^T \quad \cos(\phi/2)]$, being $\vec{e}$ and ϕ the Euler axis-angle [9] equivalent rotation from frame a to frame b.

DOI: 10.13009/EUCASS2019-657

4 Validation strategy

To validate the behaviour of the safety module during the different phases of the mission, several scenarios have been simulated using MATLAB. The sensitivity analysis includes degraded sensors, different alignments and safety configurations. The objective is to validate the safety module around the nominal values of the ALTAIR mission using Monte Carlo methods, which consist in repeating the tests several times to find the mean error. The set of parameters studied pretends to simulate a wide operational range in the frame of the Altair project but is still valid for other missions. The analysis validates the avionics configuration of other possible launchers, for instance, the quality range of the sensors simulated covers four orders of magnitude, which validates the safety module with a representative number of avionics sensors.

The different scenarios simulates a mission, including launcher and carrier. The attachment between the two bodies is considered rigid, the launcher lies attached to the carrier body frame and lies within its vertical body (except for the release phase). The simulations are divided in four phases: Pre-alignment, alignment, post-alignment and release. During the pre-alignment phase, the carrier performs a straight flight at constant wind speed. The alignment phase consist in a tach-wave manoeuver (consecution of coordinated turns to alternative sides). The final phase is the release, where the launcher starts a free fall. Before the release phase, the navigation algorithms runs using an Indirect Kalman Filter (position + velocity + attitude matching and once the launcher starts the free fall, an Extended Kalman Filter calculates the dynamic state until the end of the mission. The tests encompasses the study of several parameters, described here:

- Load Factor: Maximum ratio lift/weight of the aircraft during the manoeuvers.
- Air speed (U_∞): Velocity of the launcher wrt. the wind during the carried phases.
- Number of repetitions: Manoeuver repetitions during the alignment phase.

Base scenario

The Table 1 shows the nominal values of the parameters of interest for the sensitivity analysis and the Table 3 shows their range for this study.

Table 1: Nominal mission parameters

Parameter	Value
Air speed ($\boldsymbol{U}_\infty$)	$250\ m/s$
Load factor	3
Number of repetitions	4
Gyroscope RMSE ($\boldsymbol{\sigma_\omega}$)	$10^{-3}\ rad/s$
Accelerometer RMSE ($\boldsymbol{\sigma_a}$)	$2 \times 10^{-3}\ m/s^2$

Mission parameters sensitivity

This test consists in observing the effects on the safety assessment capabilities of the integrated system. To do so, the Table 2 shows the tests cases.

Table 2: Mission parameters sensitivity planned tests

Test case	Parameter 1	vs	Parameter 2
1	Load Factor		Air speed (U_∞)
2	Number of repetitions		Air speed (U_∞)
3	Gyroscope RMSE[a] (σ_ω)		Accelerometer RMSE[a] (σ_a)

[a]Root Mean Square Error

Results show the maximum error obtained during the exploration of each test case, which can be, depending on the output, the following assessment quantities:

- Radius of the sphere whose volume is equal to that of the 3D-ellipsoid that has the probability to contain the **quantity** estimated by the navigation/safety subsystem of 99.9%, evaluated at a specific time in the simulation. The **quantity** may be an output of navigation: position and velocity vectors in ECI or attitude error as three de-coupled small Euler angles from correct NED to erroneous NED.
- Radius of the circle whose area is equal to that of the ellipse that has the probability to contain the impact point in Mercator (aka I.P. Merc) projection estimated by the safety subsystem of 99.9%, evaluated at a specific time in simulation.
- Radius of the sphere whose volume is equal to that of the 3D-ellipsoid that has the probability to contain the **quantity** estimated by the safety subsystem of 99.9%, evaluated along at the free-fall interval in the simulation. The **quantity** may be predicted attitude error as three de-coupled small Euler angles from correct NED to erroneous NED or predicted inertial angular velocity vector in ECI.

Table 3: Ranges of the parameters of interest

Parameter	**Min value**	**Max value**	**Difference/ Ratio**	**Progression**
Air speed ($\boldsymbol{U_\infty}$)	$30\ m/s$	$250\ m/s$	$27.5\ m/s$	Arithmetic[a]
Load factor	1.5	4.5	1.25	Arithmetic[a]
Number of repetitions	1	5	1	Arithmetic[a]
Gyroscope RMSE ($\boldsymbol{\sigma_\omega}$)	$10^{-5}\ rad/s$	$0.1\ rad/s$	10	Geometric[b]
Accelerometer RMSE ($\boldsymbol{\sigma_a}$)	$2 \times 10^{-5}\ m/s^2$	$0.2\ m/s^2$	10	Geometric[b]

[a]Range obtained by arithmetic progression: the ith value is obtained as $v_i = v_{min} + (i-1)\Delta v\ \forall\ i \in 1{:}n$, where $n = 1 + (v_{max} - v_{min})/\Delta v$, v_{min} is **Min value**, v_{max} is **Max value**, and Δv is **Difference**.
[b]Range obtained by geometric progression: ith value is obtained as $v_i = v_{min} r^{i-1}\ \forall\ i \in 1{:}n$, where $n = 1 + \log_{10}(v_{max}/v_{min}) \,/\, \log_{10} r$, v_{min} is **Min value**, v_{max} is **Max value**, and r is **Ratio**

Sensor degradation

Table 4: Variable parameters of the sensor degradation

Parameter	**Possible Values**
Sensor	IMU / GNSS
Degradation factor [a]	2, 10 or NS
Time when the failure starts (considering t = 0 the start of the mission)	10, 45, 65 or 105 s

[a]A numeric value means that the RMSE associated to all the outputs of the sensor is multiplied by this value. NS means no sensor readings.

Table 5: Fixed parameters of the sensor degradation

Parameter	**Value**
Duration of the failure	10 s
Time when the alignment manoeuvre starts	40 s
Time when the alignment manoeuvre ends	60 s
Time when the launcher is released	100 s
End of the simulation	150 s

As mentioned in the previously, in addition of the parameter sensitivity exploration around Altair's nominal values, the study includes tests with a temporary malfunction of the sensors during the different phases of the mission to validate its robustness. The RMSE of the IMU and GNSS sensors are scaled up separately during a certain amount of time. Other tests deactivates the data acquisition of one sensor for the same set of periods of time. The test cases are originated from every possible permutation of the parameters in Table **4**. The timing and duration of the sensor degradation test events is specified by Table **5**. The results represent the mean error of each output at the moment of the ignition.

5 Results

The table below sums up the results for the simulations on the nominal case. Last two dynamic variables, predicted attitude and predicted angular velocity concern only the ignition consent safety algorithm. It shows the mean error at the end of each phase (at t = 40s, 60s, 100s and 150s).

Table 6 Nominal output errors

Output Errors	**Mean error**			
	Pre. Align.	Alignment	Post align.	Ignition
Attitude NED [deg]	1.011	0.132	0.038	0.052
Impact Point Mercator [m]	6.55	46.38	9.79	17.632
Position [m]	0.81	1.29	1.01	3.33
Velocity [m/s^2]	1	0.32	0.17	0.20
Predicted attitude [deg]	-	-	-	0.00073
Predicted angular velocity [rad/s]	-	-	-	0.0022

For the same dynamic variables in the table above, the next table sums up the 99.99% error radius values from the Montecarlo sensitivity study for each output:

Table 7 Maximum errors during parameters exploration

Parameters	**99.99% error radius**					
	Att. NED [deg]	I.P. Merc [m]	Pos [m]	Vel [m/s^2]	Pred. att. [deg]	Pred. ang. vel. [rad/s]
Load Factor – Air Speed	0.47	25.78	6.58	0.56	1.84	0.0064
Gyro Sigma – Acc Sigma	7.08	47.75	9.61	1.45	30.31	0.199
Load Factor - Repetitions	0.48	12.68	5.70	0.34	1.84	0.043
Repetitions – Air Speed	0.21	12.89	5.71	0.33	1.30	0.039

The next tables present the mean error at the time of ignition for different degraded scenarios, which is the most critical mission event. The results are displayed as mean error instead of 99.99% error radius because it pretends to show the sensitivity of the sensors rather than the operational range as the case of the previous tests.

Table 8 Mean errors at ignition time at degradation factor =2

		Mean error at ignition (degradation factor = 2)	
Phase when failure occurs	Dynamic variable	Sensor affected	
		GNSS	IMU
Alignment	Attitude NED [deg]	0.046	0.051
	Position [m]	3.17	3.33
	Attitude Pred NED [deg]	0.00071	0.00072
	Impact Point Merc. [m]	9.79	9.79
Post- alignment	Attitude NED [deg]	0.052	0.052
	Position [m]	3.33	3.33
	Attitude Pred NED [deg]	0.00072	0.00074
	Impact Point Merc. [m]	17.63	17.56
Release	Attitude NED [deg]	0.054	0.046
	Position [m]	3.28	3.29
	Attitude Pred NED [deg]	0.00073	0.00077
	Impact Point Merc. [m]	17.645	19.88

Table 9 Mean errors at ignition time at degradation factor =10

		Error at ignition (degradation factor = 10)	
Phase when failure occurs	Dynamic variable	Sensor affected	
		GNSS	IMU
Alignment	Attitude NED [deg]	0.052	0.051
	Position [m]	3.33	3.34
	Attitude Pred NED [deg]	0.00072	0.00071
	Impact Point Merc. [m]	19.60	19.75
Post- alignment	Attitude NED [deg]	0.046	0.051
	Position [m]	3.33	3.33
	Attitude Pred NED [deg]	0.00072	0.00072
	Impact Point Merc. [m]	19.60	20.02
Release	Attitude NED [deg]	0.083	0.114
	Position [m]	4.33	5.34
	Attitude Pred NED [deg]	0.001	0.0023
	Impact Point Merc. [m]	26.019	66.58

Table 10 Mean error at ignition time at degradation factor =NS

		Error at ignition (degradation factor = NS)	
Phase when failure occurs	Dynamic variable	Sensor affected	
		GNSS	IMU
Alignment	Attitude NED [deg]	0.047	0.54
	Position [m]	2.51	12.99
	Attitude Pred NED [deg]	0.00072	0.00080
	Impact Point Merc. [m]	13.38	9.55
Post- alignment	Attitude NED [deg]	0.046	0.060
	Position [m]	2.53	2.72
	Attitude Pred NED [deg]	0.00070	0.00068
	Impact Point Merc. [m]	14.11	9.44
Release	Attitude NED [deg]	0.040	1.80
	Position [m]	2.42	4.2
	Attitude Pred NED [deg]	0.00077	0.0053
	Impact Point Merc. [m]	11.63	59.18

6 Conclusions and future work

The classic approach of the ground safety based on human decision chain relies on the information obtained from redundant sources of the launcher dynamic. The challenge of the on-board flight safety relies in the real-time performance of the autonomous decision-making based only on the on-board navigation instruments. The work assess the performance, robustness and precision, of the real-time safety algorithms in synergy with the navigation nominal and degraded scenarios with the objective of validating the operational mission frame of the AOBFS approach.

The IMU sensor is very robust during pre-alignment and post-alignment phase, the increase of error or even the lack of data during a short period of time do not affect the navigation nor safety performance. Nevertheless, if the sensor data is degraded during the alignment or ballistic phase (in-flight safety), the effect is an increase of navigation errors that do not decrease in a short-term period after the sensor recovering. The navigation solution do not reach the minimum possible levels and therefore the safety algorithms are based on degraded data and therefore the safety solution is also degraded. In future studies, a data quality filter shall be considered in order to protect a critical system such as the AOBFS from degraded information, weighing in the filters the affected sensor with higher weight and so rely only launcher IMU data in front of degraded scenarios. Regarding the GNSS sensor, during the phase where it works (ballistic), the degradation influences considerably to the navigation and safety subsystems especially if the avionics does not know that the sensor is giving wrong data. On the other hand, once the sensor is recovered, the errors

are reduced to nominal levels within seconds (with 10 s of degradation the error levels recover its nominal level after 60 s).

The precisions obtained from safety algorithms, ground impact and attitude prediction, in nominal and degraded scenarios validate the approach of a real-time flight safety and its appropriateness for on-board autonomous safety decision making. The robustness of safety algorithms it is not affected by hybrid navigation strategies, allowing the niche of micro launchers the use of low-cost and light weight navigation instruments without loss of safety performance. However, the processing of navigation data shall be improved in terms of quality since safety algorithms are sensitive to degraded information: it is preferable the lack of information rather than the use of uncertain information that may lead to a unreliable safety output. The AOBFS system is planned to be tested in real-flight in the frame of the ALTAIR project in test campaigns at the European spaceport in French Guyana (CSG)

References

[1] K. Davidian, S. Isakowitz, J. Logsdon, J. R. McMurry, G. Nield and M. S. Smith. 2013. Growing the Future of Commercial Space. *New Space.* 1(1):3-9.

[2] B. Doncaster, C. Williams and J. Shulman. 2017. 2017 Nano/Microsatellite Market Forecast. SpaceWorks Enterprises, Inc. (SEI). Atlanta, GA.

[3] D. Vallverdú, C. Pou, M. Badenas and E. Diez. 2018. A Real-Time Hybrid Navigation System for an Autonomous Space Launch Vehicle. In *9th Embedded Real Time Software and Systems (ERTS) European Congress*.

[4] W. E. Wiesel. 2010. Modern orbit determination. 2nd ed.. Beavercreeck. Ohio: Aphelion Press.

[5] Y. Liu, X. Fan, C. Lv, J. Wu, L. Li and D. Ding. 2018. An innovative information fusion method with adaptive Kalman filter for integrated INS/GPS navigation of autonomous vehicles. *Mechanical Systems and Signal Processing.* 100:605-616.

[6] D. H. Titterton and J. L. Weston. 2004. Strapdown inertial navigation technology. Vol. 17. IET.

[7] Y. Yüksel. 2005. Design and analysis of transfer alignment algorithms. PhD Thesis. Middle East Technical University.

[8] A. Tromba et al. ALTAIR Orbital Module Preliminary Mission and System Design. EUCASS 2017

[9] Gary W. Hunter et al. A concept of operations for an IVH assurance system. NASA/TM-March 2013.

[10] X. Tang, Z. Liu, and J. Zhang, "Square-root quaternion cubature Kalman filtering for spacecraft attitude estimation," *Acta Astronaut.*, vol. 76, no. July 2012, pp. 84–94, Jul. 2012.

[11] S. J. Julier and J. K. Uhlmann, "Unscented Filtering and Nonlinear Estimation," *Proc. IEEE*, vol. 92, no. 3, pp. 401–422, Mar. 2004.

[12] J. F. Kuzanek, "Improved Methods for Computing Drag Corrected Missile Impact," in *Army Science Conference*, 1980, vol. 2, pp. 381–393

[13] N. Trawny and S. I. Roumeliotis, "Technical Report: Indirect Kalman filter for 3D Attitude Estimation," Multiple Autonomous Robotic Systems Laboratory, University of Minnesota, Minneapolis, MN, USA, 2005.

[14] M. S. Grewal, L. R. Weill, and A. P. Andrews, *Global Positioning Systems, Inertial Navigation, and Integration*, 2nd ed. Hoboken, NJ, USA: John Wiley & Sons, Inc., 2007.

[15] A. Solimeno, "Low-Cost INS / GPS Data Fusion with Extended Kalman Filter for Airborne Applications," Universidade Técnica de Lisboa, 2007.